Supplemental Materials

Elastomer Grafted iPSC-Derived Micro Heart Muscles to Investigate Effects of Mechanical Loading on Physiology

Jingxuan Guo[1], Daniel W. Simmons[2,3], Ghiska Ramahdita[1], Mary K. Munsell[2], Kasoorelope Oguntuyo[2], Brennan Kandalaft[2], Brandon Rios[2], Missy Pear[2], David Schuftan[2], Huanzhu Jiang[2], Spencer P. Lake[1], Guy M. Genin[1-3], Nathaniel Huebsch[2-4]

1. Department of Mechanical Engineering and Material Science
2. Department of Biomedical Engineering
3. NSF Science and Technology Center for Engineering Mechanobiology
4. Center for Cardiovascular Research, Center for Regenerative Medicine, Center for Investigation of Membrane Excitability Diseases, Washington University in Saint Louis

Corresponding author: Nathaniel Huebsch, PhD, Campus Box 1097, 1 Brookings Drive, Saint Louis, MO, 63130

Telephone: (314) 935-3534

Email: nhuebsch@wustl.edu

Supplemental Methods

PDMS-C2C12 Cellular Adhesion Response

Cell adhesion assays using C2C12 myoblast cell line, were performed to test the bioactivity of PDMS-grafted FN. FN-coated tissue culture polystyrene was used as a positive control and FN was diluted into dPBS and applied at saturating density (20 μg/mL; supplemental Figure 2)[1]. Followed by the FN washing steps described in section 2.3 in the main text, the surfaces were then disinfected with 70% ethanol for at least 2.5 hours, then washed 3 times with sterile dPBS and stored at room temperature for up to 24 hours before cell culture studies.

C2C12 myoblasts were plated at 5,000 cells/cm^2 in Dulbecco's Modified Eagle Medium (DMEM; Thermo Fisher Scientific) with 1% fetal bovine serum (FBS; Thermo Fisher Scientific). After 2 hours incubation at 37ºC with 5% CO_2, the cells were washed gently 3 times with dPBS and fixed using 4% paraformaldehyde. To quantify cell adhesion and spreading, cells were permeabilized with 0.1% Triton-X-100 and stained with Alexa Fluor 488 Phalloidin (30 minutes to mark F-actin). Multiple fluorescence images were then taken for each test condition using an epifluorescence microscope (Nikon Eclipse Ts2R), and individual projected cell areas were quantified using ImageJ.

C2C12 Micro-Skeletal Muscle (μSM) Formation

To evaluate whether ECM grafted surfaces can enhance tissue stability and prevent tissue from collapsing, C2C12 myoblasts cell line, was used to form micro-skeletal muscles (μSM). C2C12 myoblast was seeded into "dog bone" shaped PDMS stencils atop Sylgard 527 substrates. After surface treatment and stencil mold assembly atop the substrate, 5 μg/mL of FN was coated, followed by washing, quenching and disinfection steps. C2C12 (5 x 10^7/mL) were applied in a 3 μL volume (total of 1.5 x 10^5 cells) to fill each "dog bone" shaped stencil mold (Supplemental Figure S4 A). Seeded cells were incubated for 2 hours at 37ºC with 5% CO_2 before adding DMEM with 5% FBS. The incubation step is to help prevent cells from shearing/floating off the substrates when adding media. Seeded μSM were monitored for collapse and detachment daily over one week. Tissue stability was quantified using tissue occupied area, calculated by dividing tissue area by the total mold area. Area of the tissue and mold were measured using ImageJ. At least three representative tissues were measured.

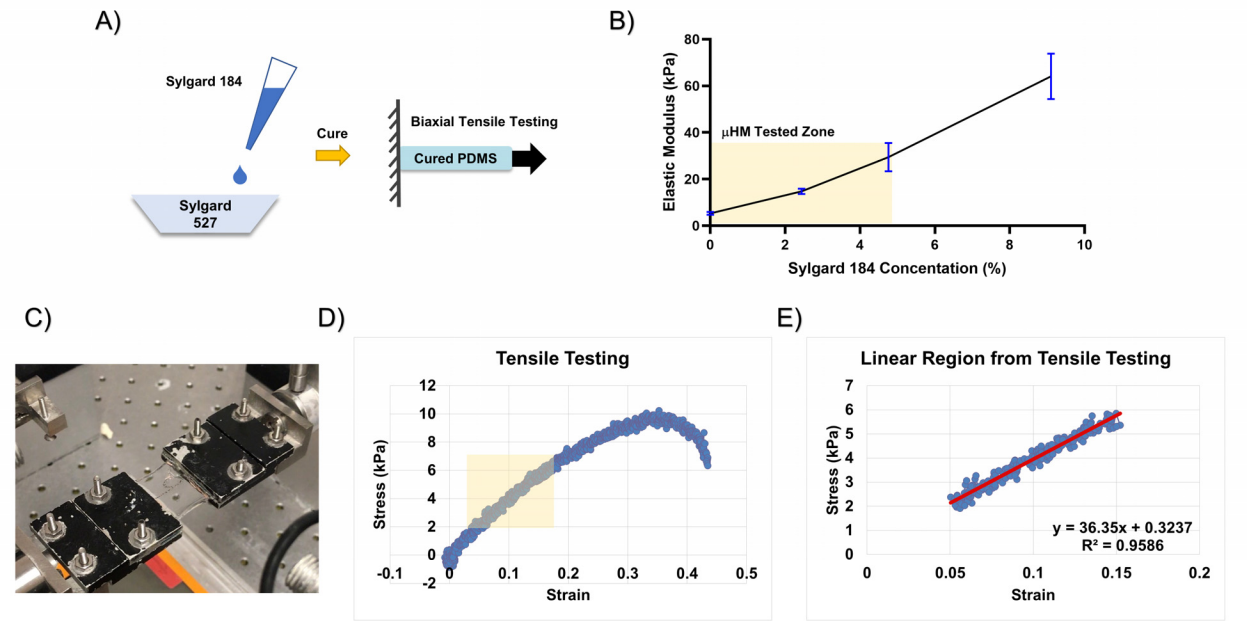

Figure S1. Tensile Testing to Characterize of PDMS Elasticity. A) Modulating elastomer properties by adding different amount of Sylgard 184 into Sylgard 527, uniaxial tensile testing was performed to determine material properties[2]. **B)** Elasticity quantification of different PDMS mixtures, highlighted area indicating 5 to 30 kPa elasticity was chosen for iPSC-μHM study. **C)** Planar biaxial testing machine setup[3]. PDMS strips were clamped onto two load cells for uniaxial tension test. One of the actuators move at a constant 1 mm/s speed to stretch the PDMS, while the load cell recorded force and elongation. **D)** Stress vs strain curve for a PDMS sample tensile test until failure, linear region (yellow highlight) is extracted. **E)** Linear regions of the stress vs strain curves were used to get elasticity. Error bars: standard deviation (*SD)*, *n* >10 (B).

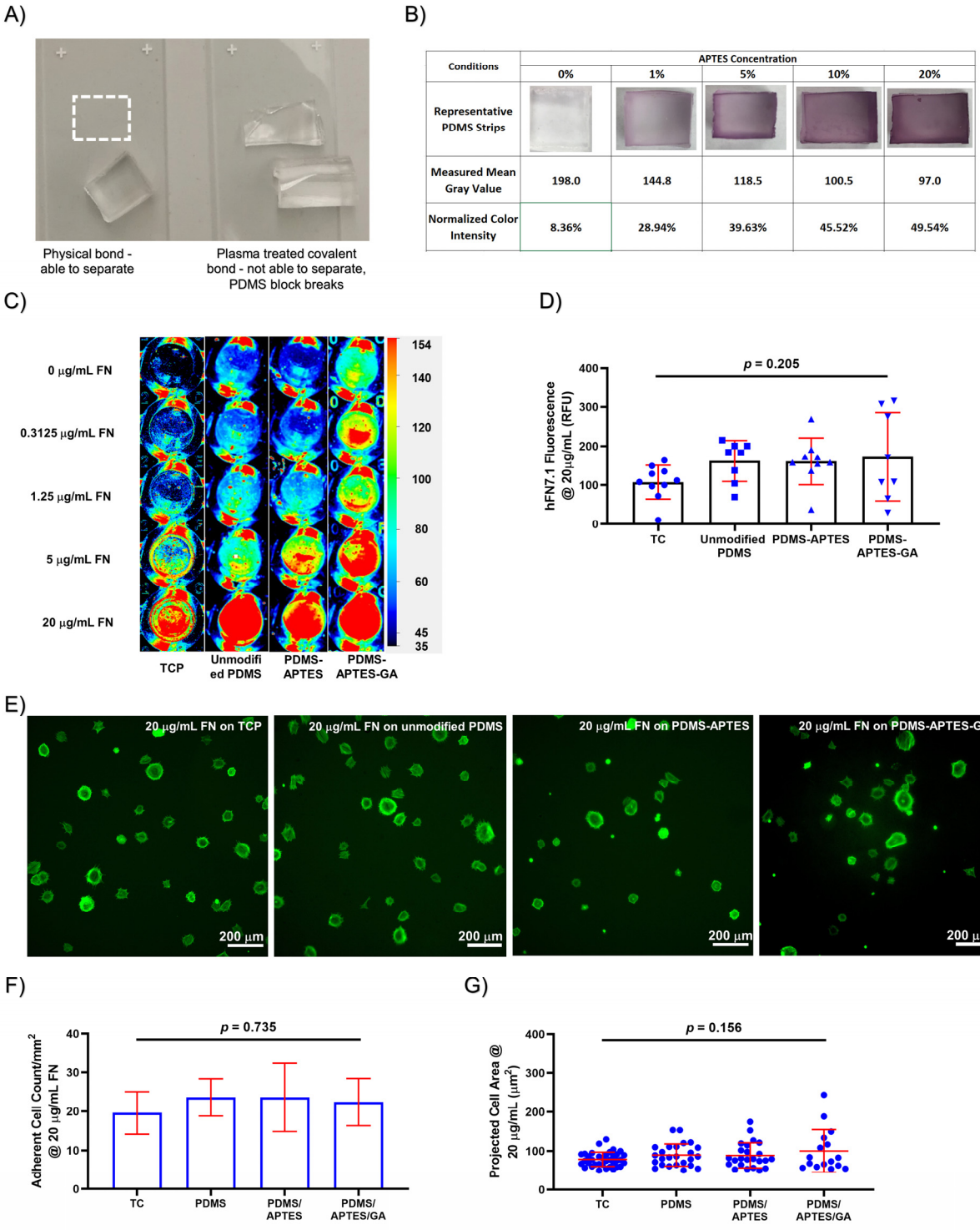

Figure S2. Surface Characterization. A) Physical bond of PDMS and glass shown in left figure, PDMS strip was able to be removed from glass; successful plasma reaction will covalently bind PDMS and glass slides together (right figure), forced separation will cause PDMS to break. **B)** Representative images of ninhydrin colorimetric reaction upon APTES reaction[4]. **C)** Representative Li-cor scanning image of hFN 7.1 antibody intensity on different PDMS surfaces at different FN concentrations. As FN concentration increases, hFN 7.1

fluorescence intensity increase, PDMS-APTES and PDMS-APTES-GA surfaces have qualitatively higher intensity, 0 μg/mL FN was used to extract from measured mean fluorescence intensity to eliminate autofluorescence of different surfaces. **D)** hFN 7.1 fluorescence intensity on different surfaces when coated with 20 μg/mL FN, one-way ANOVA indicates no significant difference between surfaces. **E)** Representative Phalloidin stain image of C2C12 cell spreading on different surfaces, left to right: TCP, unmodified PDMS, PDMS-APTES, and PDMS-APTES-GA. **F)** Adherent C2C12 cell number per mm^2 for different surfaces coated with 20 μg/mL FN, no significant difference was observed (p = 0.735) **G)** C2C12 projected area quantification on different surfaces coated with 20 μg/mL FN, no significant difference in cell spread area was observed between different surfaces (p = 0.156). Error bar: *SD*.

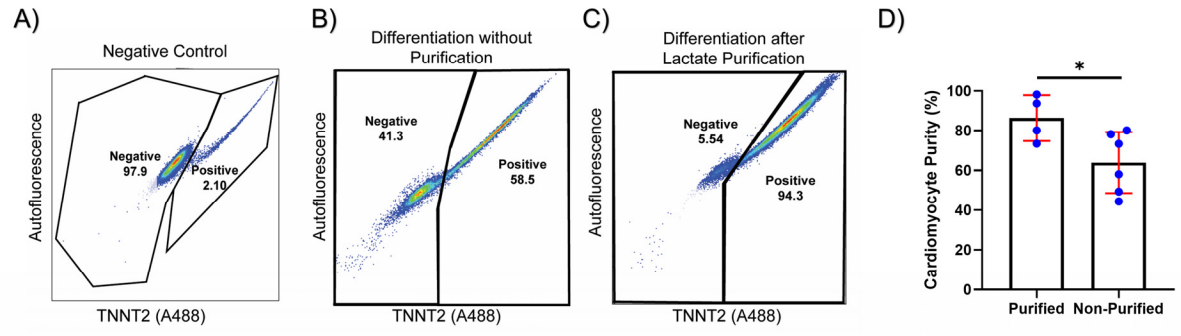

Figure S3. Quantification of Cardiomyocyte Purity. A) Representative negative control images of flow cytometry quantification of iPSC-cardiomyocyte purity (cTnT antibody, 13-11), cells from non-beating walls after iPSC differentiation were used for negative control. **B)** Representative flow cytometry quantification of non-purified cardiomyocytes directly after iPSC differentiation. **C)** Representative flow cytometry quantification image of cardiomyocytes treated with lactate media for 4 days[5]. **D)** Quantification of flow cytometry data on different purified and non-purified batches. Cardiomyocytes purity is statistically significant between purified and non-purified (p value = 0.03). Purified cardiomyocytes batches used in this study has the average purification of 86%. * indicates $p < 0.05$, Error bar: *SD*.

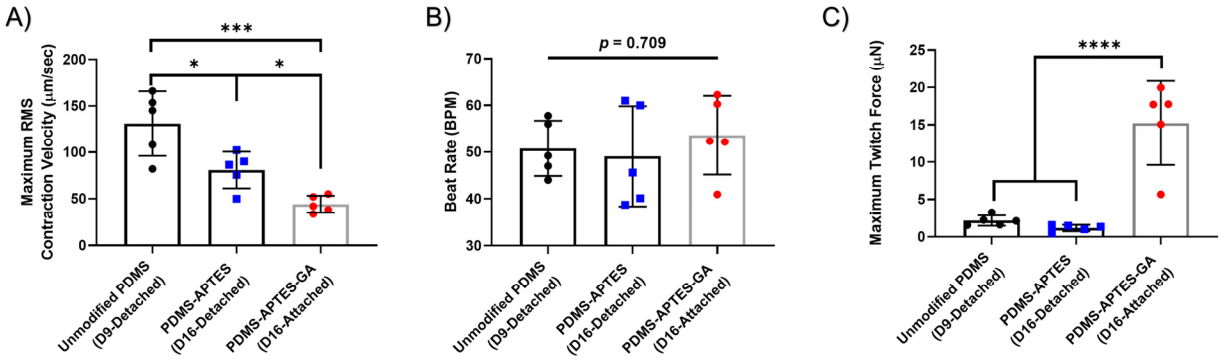

Figure S4. Tissue Detachment Analysis using Motion Tracking Algorithm and TFM Algorithm. A) Contraction velocity of tissues formed on unmodified PDMS (Day 9-detached), PDMS-APTES (Day 16-detached), and PDMS-APTES-GA (Day 16-attached), motion was detected for all tissues, high tissue contraction velocity indicating tissue contract freely without doing mechanical work against substrate (resistance). Attached tissue (PDMS-APTES-GA) has significant lower contraction velocity compared to collapsed tissue (unmodified PDMS, p = 0.0003, PDMS-APTES, p = 0.03) **B)** Beat rate for tissues formed on different substrates, no significant difference was seen on different surfaces (p = 0.709). **C)** Traction force analysis of the fluorescent beads motion, not much motion of the beads was detected on detached tissue (on unmodified PDMS and PDMS-APTES), while traction was detected for PDMS-APTES-GA tissues. *. *** and **** indicates $p < 0.05$, 0.001, and 0.0001, respectively. Error bar: *SD*.

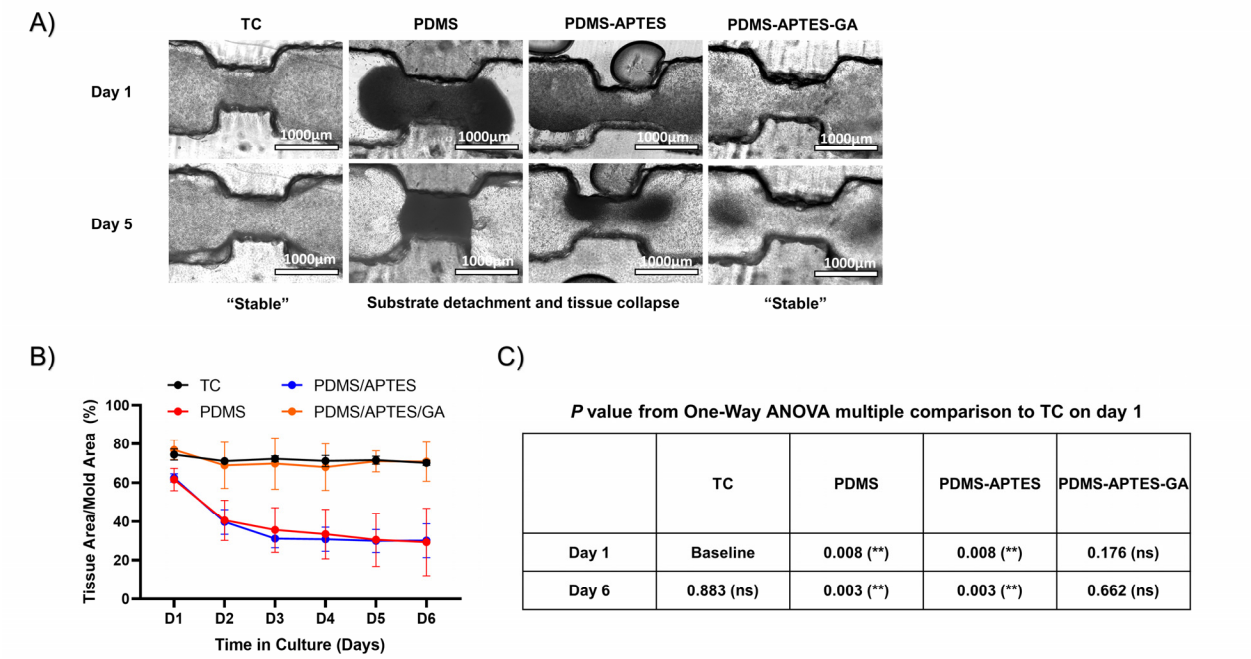

	TC	PDMS	PDMS-APTES	PDMS-APTES-GA
Day 1	Baseline	0.008 (**)	0.008 (**)	0.176 (ns)
Day 6	0.883 (ns)	0.003 (**)	0.003 (**)	0.662 (ns)

Figure S5. Consistent C2C12 Micro-Skeletal Muscle (µSM) Formation on Modified PDMS Substrates. A) Representative micrographs of C2C12 micro tissue formation on different substrates at 1 and 5 days after seeding. **B)** Quantification of collapse of C2C12 micro tissues over the first 6 days of culture; for TC and PDMS-APTES-GA, C2C12 µSM are "stable" compared with unmodified PDMS and APTES modified PDMS, where tissues tend to collapse. **C)** Statistical analysis of the quantified data, both unmodified PDMS and APTES modified PDMS are significantly collapsed compared with positive control, while PDMS-APTES-GA is similar to the positive control. Scale bars: B: 1000 µm. Error bars: *SD*, *n* =3.

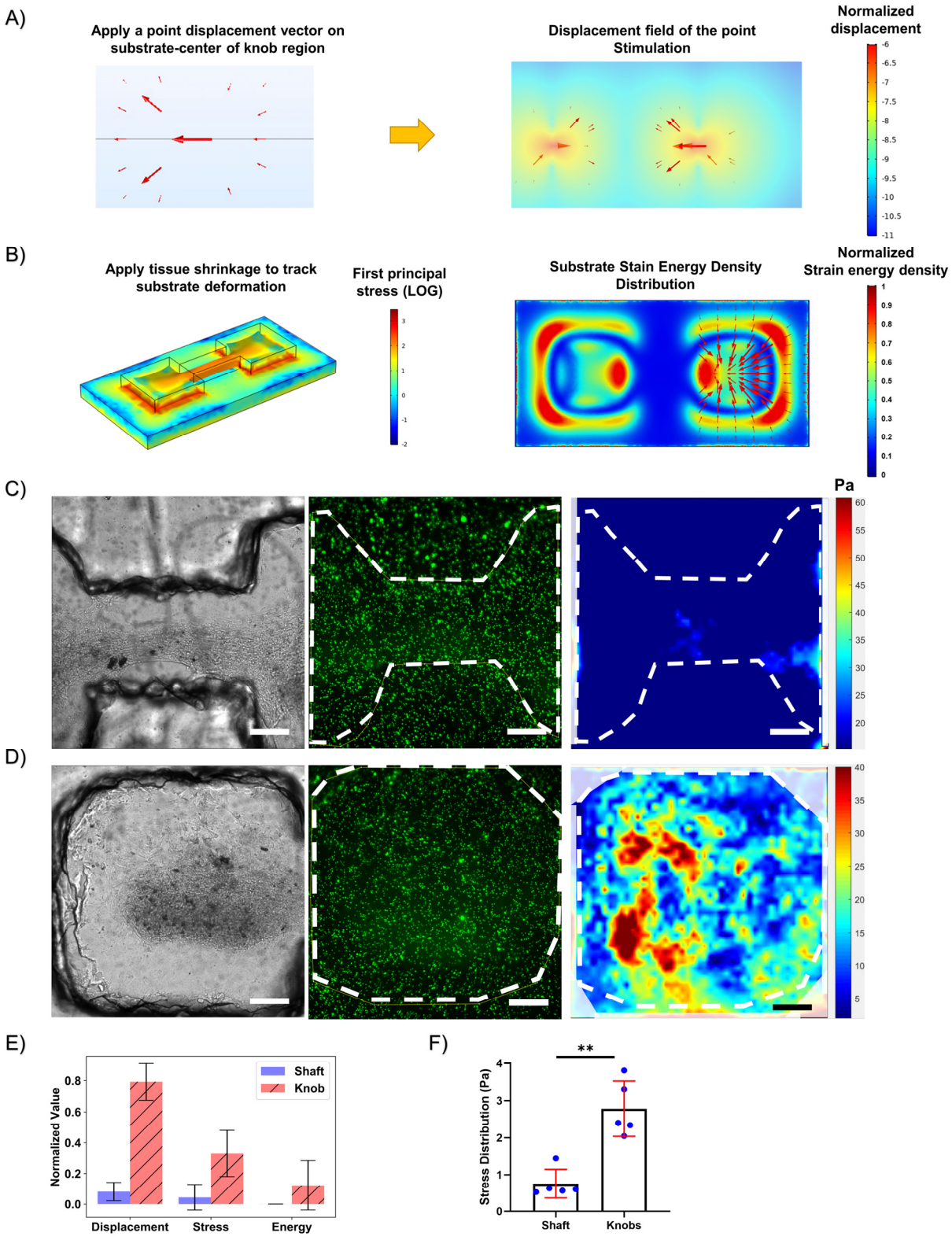

Figure S6. Finite Element Analysis of Shaft vs. Knob Regions of the TFM Substrates. A) Point stimulation using a displacement vector in the middle of the knob regions to visualize substrate deformation, substrate displacement field (right) indicating majority of the motion was

in the middle of the knob regions and expanded in the surrounding areas close to the “dog-bone” regions while minimal motion was seen at shaft region. **B)** Tissue contraction simulation (using 1% shrinkage of tissue, left panel) to visualize substrate deformation, results indicating majority of deformation happens on the edges of the knob regions and on the shoulders of the shaft region. **C-D)** Representative images of TFM experiment data for shaft regions (C) and knob regions (D), from left to right: bright field tissue image, fluorescence beads image and computed traction force heatmap (color scale unit: Pa), traction heat map indicating minimal force were observed in the middle of the shaft region. **E)** FEA simulation results quantified at shaft vs knob regions (normalized by maximum value) indicates much less displacement, stress and energy in the shaft regions compared to knob regions. **F)** Experimental TFM quantification of stress distribution on shaft vs knob regions, significant higher stress was shown in knob regions. These results indicate knob regions, where tissue fully attached can better represent tissue contractility (p = 0.0016). Scale bars: C-D: 200 μm, G: 500 μm. ** indicates $p < 0.01$. Error bar: *SD*.

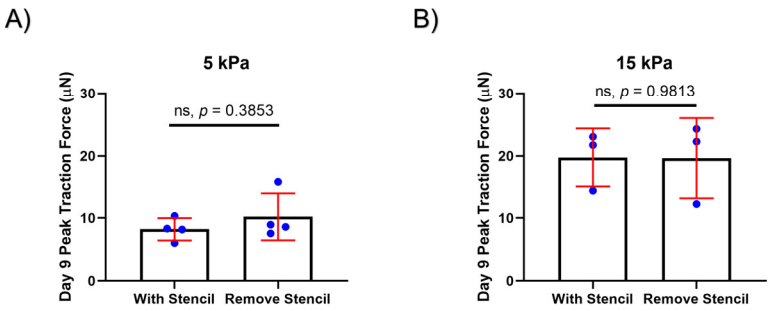

Figure S7. iPSC-μHM Contractility with and without Stencil atop Soft Substrate at Day 9. Stencil mold effects on tissue contractility was validated by carefully removing stencil at day 9. TFM was recorded before and after stencil removal. **A)** Contractility of iPSC-μHM on 5 kPa substrate at day 9, no significant difference was found with or without stencil, *p* value 0.3853. **B)** Contractility of iPSC-μHM on 15 kPa substrate at day 9, no significant difference was found with or without stencil, *p* value 0.9813.

A)

	Averaged Tissue occupied area in knob regions (mm²)
Day 9	0.48 mm²
Day 16	0.34 mm²

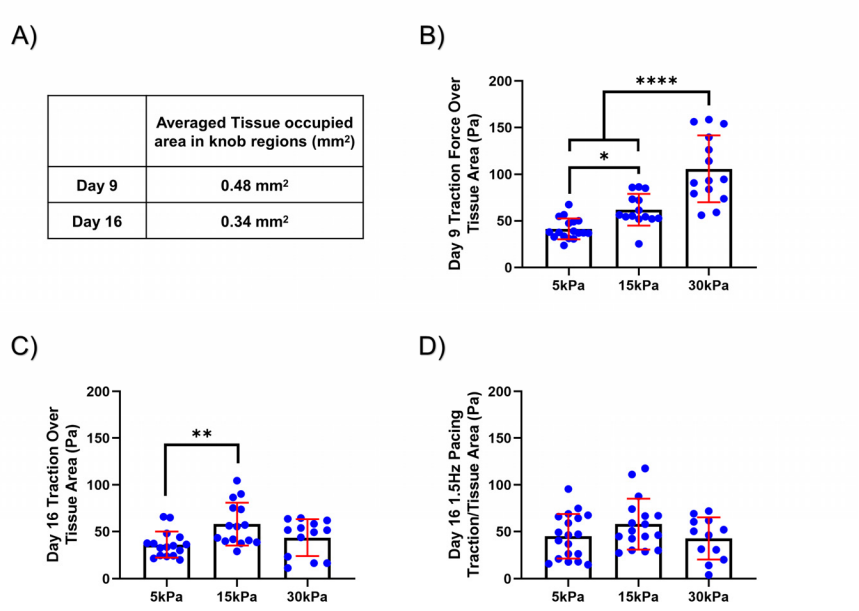

Figure S8. iPSC-μHM Stress Generation (Traction per unit tissue area) on Day 9 and Day 16. A) Average tissue occupied area in knob regions on day 9 and day 16, a decrease in area indicates potential tissue compaction over time[6]. **B)** Day 9 tissue traction force generated per unit area, 30 kPa tissue generate most stress (contraction over area) compared to 5 and 15 kPa tissues ($p < 0.0001$), 15 kPa tissue also has significantly higher stress than 5 kPa ($p = 0.018$). **C)** Day 16 spontaneous contraction force per unit area. Compared to day 9, there is no significant change of unit contractility for 5 kPa ($p = 0.861$) and 15 kPa ($p = 0.875$), however, a significant amount of unit contractility decrease for 30 kPa from day 9 to day 16 ($p < 0.0001$). Meanwhile, 15 kPa μHM generates significantly higher stress than 5 kPa μHM ($p = 0.008$). **D)** Day 16 1.5 Hz field pacing tissue traction force per unit area. One-way ANOVA indicates no significant difference between groups ($p = 0.182$). No significant difference was found between spontaneous contractility vs 1.5 Hz pacing for 5 kPa ($p = 0.861$),15 kPa ($p = 0.995$) and 30 kPa ($p = 0.938$). ****, ** and * indicates $p < 0.0001$, 0.01 and 0.05, respectively. Error bar: *SD*.

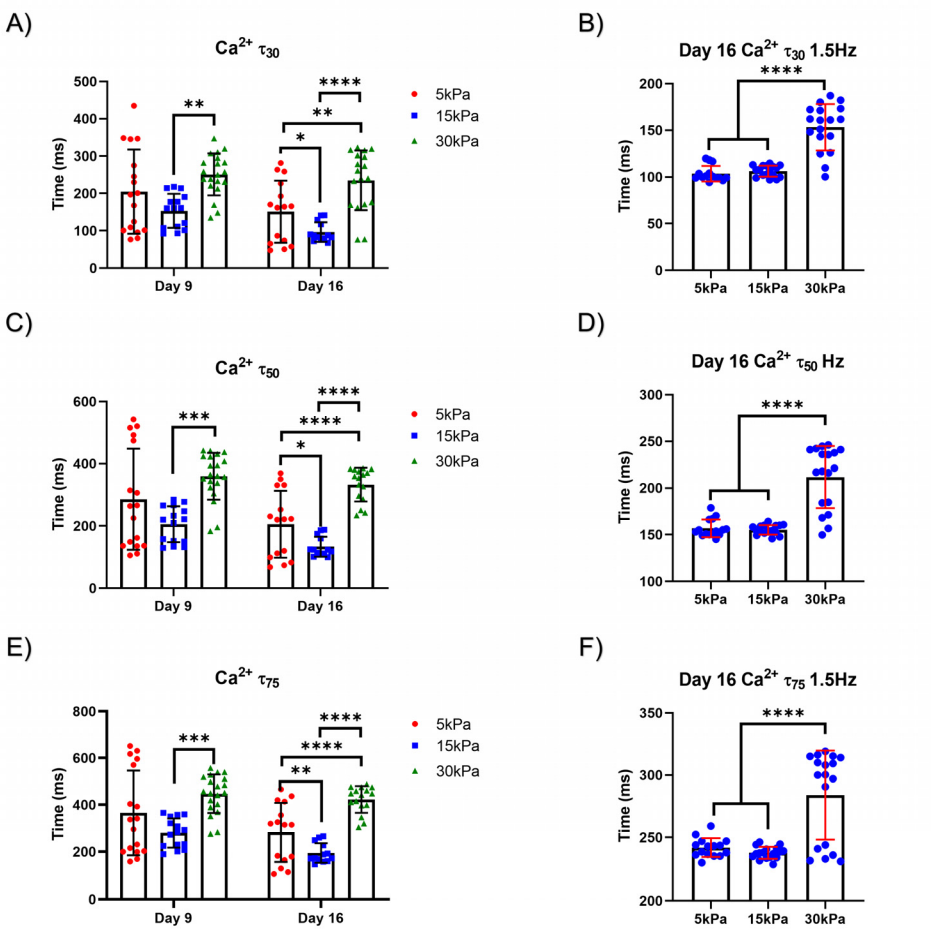

Figure S9. iPSC-μHM Day 9 and Day 16 Calcium Decay Times. A-B) Calcium τ_{30} at spontaneous beating and 1.5 Hz field pacing. **C-D)** Calcium τ_{50} at spontaneous beating and 1.5 Hz pacing. **E-F)** Calcium τ_{75} at spontaneous beating and 1.5 Hz pacing. Based on beat rate corrected calcium decay values[7], 15 kPa μHM has significant lower decay values compared to 30 kPa μHM on day 9, this trend become more significant on day 16. We observed calcium decay time decrease over time (two-way ANOVA indicates time factor $p < 0.0001$). At 1.5 Hz pacing. 30 kPa μHM decay times are significant longer compared to 5 and 15 kPa tissues ($p < 0.0001$). Compared to spontaneous beating, calcium decay times decreases at 1.5 Hz pacing. ****, ***, ** and * indicates significant difference $p < 0.0001$, 0.001, 0.01 and 0.05, respectively. Error bars: *SD*.

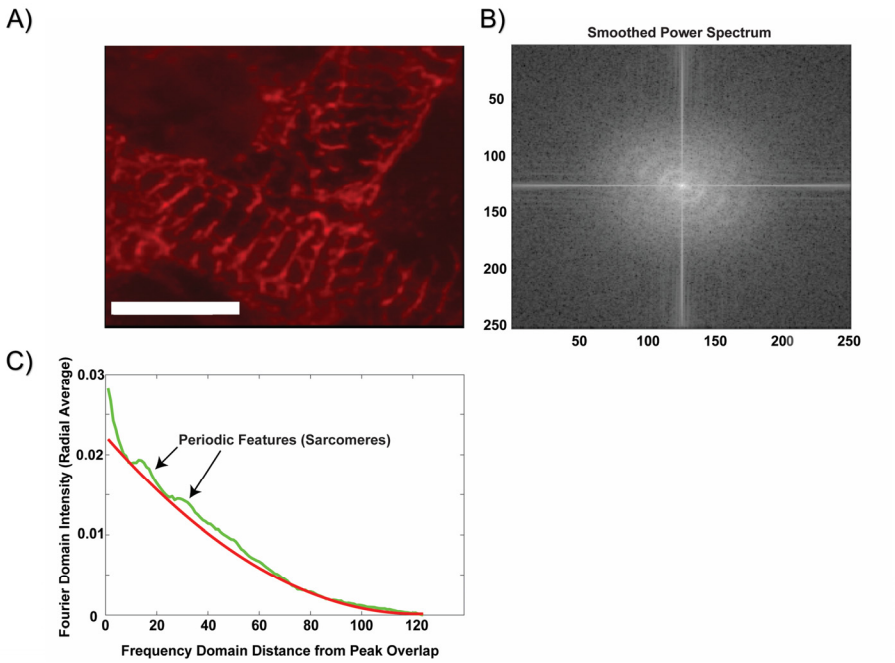

Figure S10. Sarcomere Regularity Quantification using Fourier Analysis. A) Regions of Sarcomere that was selected for Fourier analysis (5 kPa μHM). **B)** Fast Fourier Transform (FFT)[8] was used to generate smoothed power spectrum based on selected sarcomere regions. **C)** Fourier domain intensity representing regularity of the sarcomere, upon subtracting background signal, the Fourier domain intensity for sarcomere picks were identified. Scale bar: 10 μm.

References

(1) García, A. J., Vega, M. D., & Boettiger, D. Modulation of Cell Proliferation and Differentiation through Substrate-Dependent Changes in Fibronectin Conformation. *Mol. Biol. Cell* **1999**, *10* (3), 785–798. https://doi.org/10.1016/j.cpc.2005.06.001.

(2) Palchesko, R. N.; Zhang, L.; Sun, Y.; Feinberg, A. W. Development of Polydimethylsiloxane Substrates with Tunable Elastic Modulus to Study Cell Mechanobiology in Muscle and Nerve. *PLoS One* **2012**, *7* (12). https://doi.org/10.1371/journal.pone.0051499.

(3) Eekhoff, J. D.; Fang, F.; Kahan, L. G.; Espinosa, G.; Cocciolone, A. J.; Wagenseil, J. E.; Mecham, R. P.; Lake, S. P. Functionally Distinct Tendons from Elastin Haploinsufficient Mice Exhibit Mild Stiffening and Tendon-Specific Structural Alteration. *J. Biomech. Eng.* **2017**, *139* (11), 1–9. https://doi.org/10.1115/1.4037932.

(4) Ribeiro, A. J. S.; Zaleta-Rivera, K.; Ashley, E. A.; Pruitt, B. L. Stable, Covalent Attachment of Laminin to Microposts Improves the Contractility of Mouse Neonatal Cardiomyocytes. *ACS Appl. Mater. Interfaces* **2014**, *6* (17), 15516–15526. https://doi.org/10.1021/am5042324.

(5) Tohyama, S.; Hattori, F.; Sano, M.; Hishiki, T.; Nagahata, Y.; Matsuura, T.; Hashimoto, H.; Suzuki, T.; Yamashita, H.; Satoh, Y.; Egashira, T.; Seki, T.; Muraoka, N.; Yamakawa, H.; Ohgino, Y.; Tanaka, T.; Yoichi, M.; Yuasa, S.; Murata, M.; Suematsu, M.; Fukuda, K. Distinct Metabolic Flow Enables Large-Scale Purification of Mouse and Human Pluripotent Stem Cell-Derived Cardiomyocytes. *Cell Stem Cell* **2013**, *12* (1), 127–137. https://doi.org/10.1016/j.stem.2012.09.013.

(6) Wang, E. Y.; Rafatian, N.; Zhao, Y.; Lee, A.; Lai, B. F. L.; Lu, R. X.; Jekic, D.; Davenport Huyer, L.; Knee-Walden, E. J.; Bhattacharya, S.; Backx, P. H.; Radisic, M. Biowire Model of Interstitial and Focal Cardiac Fibrosis. *ACS Cent. Sci.* **2019**, *5* (7), 1146–1158. https://doi.org/10.1021/acscentsci.9b00052.

(7) Fridericia, L. S. The Duration of Systole in an Electrocardiogram in Normal Humans and in Patients with Heart Disease. *Ann. Noninvasive Electrocardiol.* **2003**, *8* (4), 343–351. https://doi.org/10.1046/j.1542-474X.2003.08413.x.

(8) Ma, Z.; Huebsch, N.; Koo, S.; Mandegar, M. A.; Siemons, B.; Boggess, S.; Conklin, B. R.; Grigoropoulos, C. P.; Healy, K. E. Contractile Deficits in Engineered Cardiac Microtissues as a Result of MYBPC3 Deficiency and Mechanical Overload. *Nat. Biomed. Eng.* **2018**, *2* (12), 955–967. https://doi.org/10.1038/s41551-018-0280-4.